Progress In Electromagnetics Research B, Vol. 2, 27–60, 2008

AN INTRODUCTION TO SYNTHETIC APERTURE RADAR (SAR)

Y. K. Chan and V. C. Koo

Faculty of Engineering & Technology
Multimedia University
Jalan Ayer Keroh Lama, Bukit Beruang, 75450 Melaka, Malaysia

Abstract—This paper outlines basic principle of Synthetic Aperture Radar (SAR). Matched filter approaches for processing the received data and pulse compression technique are presented. Besides the SAR radar equation, the linear frequency modulation (LFM) waveform and matched filter response are also discussed. Finally the system design consideration of various parameters and aspects are also highlighted.

1. INTRODUCTION

Radar has long been used for military and non-military purposes in a wide variety of applications such as imaging, guidance, remote sensing and global positioning [1]. Development of radar as a tool for ship and aircraft detection was started during 1920s. In 1922, the first continuous wave radar system was demonstrated by Taylor. The first pulse radar system was developed in 1934 with operating frequency 60 MHz by Naval Research Laboratory (NRL), US. At the same time, radar systems for tracking and detection of aircraft were developed both in Great Britain and Germany during the early 1930s.

The first imaging radar, developed during World War II, used the B-Scan which produced an image in a rectangular format. The nonlinear relation between angle and distance to the side of aircraft produced great distortions on the display. This distortion was greatly improved by development of Plan Position Indicator (PPI). Its antenna beam was rotated through 360° about the aircraft and a picture of ground was produced. In the 1950s, the Side Looking Airborne Radar (SLAR) was developed. Scanning had been achieved with the SLAR by fixed beam pointed to the side with aircraft's motion moving the beam across the land. The early versions of SLAR systems were primarily used for military reconnaissance purposes. Until mid 1960s, the first

high-resolution SLAR image was declassified and made available for scientific use.

However, the image formed by SLAR is poor in azimuth resolution. For SLAR the smaller the azimuth beamwidth, the finer the azimuth resolution. In order to obtain high-resolution image one has to resort either to an impractically long antenna or to employ wavelengths so short that the radar must contend with severe attenuation in the atmosphere. In airborne application particularly the antenna size and weight are restricted. Another way of achieving better resolution from radar is signal processing. Synthetic Aperture Radar (SAR) is a technique which uses signal processing to improve the resolution beyond the limitation of physical antenna aperture [2]. In SAR, forward motion of actual antenna is used to 'synthesize' a very long antenna. SAR allows the possibility of using longer wavelengths and still achieving good resolution with antenna structures of reasonable size.

In 1952, "Doppler beam-sharpening" system was developed by Wiley of Goodyear Corporation. This system was not side looking radar. It operated in squint mode with the beam point around 45° ahead. The radar group at Goodyear research facility in Litchfield, Arizona pursued Wiley's concept and built the first airborne SAR system, flown aboard a DC-3 in 1953. The radar system operated at 930 MHz, used a Yagi antenna with real aperture beamwidth of 100°. During the late 1950s, and early 1960s, classified development of SAR systems took place at the University of Michigan and at some companies. At the same time, similar developments were conducting in other country such as Russia, France and United Kingdom.

The use of SAR for remote sensing is particularly suited for tropical countries. By proper selection of operating frequency, the microwave signal can penetrate clouds, haze, rain and fog and precipitation with very little attenuation, thus allowing operation in unfavourable weather conditions that preclude the use of visible/infrared system [3]. Since SAR is an active sensor, which provides its own source of illumination, it can therefore operate day or night; able to illuminate with variable look angle and can select wide area coverage. In addition, the topography change can be derived from phase difference between measurement using radar interferomentry. SAR has been shown to be very useful over a wide range of applications, including sea and ice monitoring [4], mining [5], oil pollution monitoring [6], oceanography [7], snow monitoring [8], classification of earth terrain [9] etc. The potential of SAR in a diverse range of application led to the development of a number of airborne and spaceborne SAR systems.

Some SAR systems are described as follow. A polarimetric airborne SAR system was developed by NASA Jet Propulsion Laboratory (JPL) and loaded on CV-990 aircraft system [10]. The radar was operated at a wavelength of 24.5 cm (L-band) and had a 4-look resolution of about 10 m by 10 m. In July 1985, the CV-990 together with the SAR instrumentation was destroyed by fire during an aborted takeoff from March Air Force Base in Southern California. After the disaster, a new imaging radar (AIRSAR) was built at JPL and this system incorporates all the characteristics of the previous CV-990 L-band SAR. Fig. 1.1 shows the basic block diagram of the CV-990 system. The CV-990 system employed two separate antennas, one horizontally polarised and the other vertically polarised. Full polarisation can be achieved by transmits a pulses train through the switching circuitry. The pulses are transmitted through horizontal polarised antenna and received signal from both antenna. Then followed by transmits vertical polarised pulse and received by both antenna. Circulators permit a single antenna to be used for both transmission and reception. The CV-990 radar has served as the prototype for all other currently operating imaging radar and for the spaceborne system proposed by NASA for operation in 1990s.

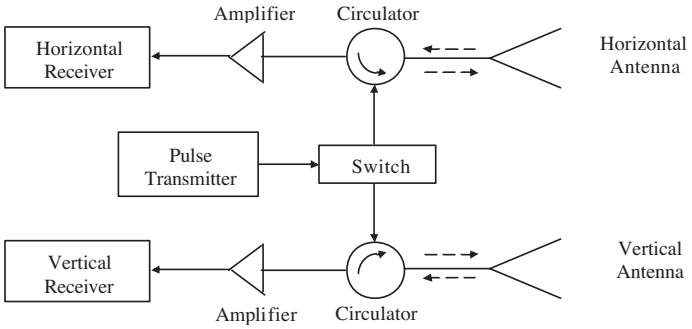

Figure 1.1. Basic block diagram of the CV-990 polarimetric SAR system.

The AIRSAR system was built based on CV-990 L-band SAR and extended to include P-Band (440 MHz) and C-band (5300 MHz) [11]. The new system is capable of producing fully polarimetric data from all three frequencies simultaneously. It collects HH, HV, VH and VV data at all three frequencies with approximately 10 m resolution. Fig. 1.2 shows the functional diagram of AIRSAR. The system has a single stable local oscillator (STALO) clock and a single exciter source, which operates at L-Band. Each generated chirp is up-converted to C-Band and down-converted to P-Band. Each of the P- and L-Band signal is

amplified by a travelling wave tube (TWT). For C-Band, 2 TWTs are used before the signal is split into H and V channels for transmission. The H and V transmission events are separated in time by half a pulse repetition interval. The TWTs give peak power outputs of 6 kW at L-Band and 1 kW at P- and C-Band. A wide dynamic range is achieved by using 8-bit analogue-to-digital converters (ADC's). The ADC's each operates at 45 MHz and produces real-data samples (not I and Q) at a total data rate of between 20 and 60 Mbytes/second. The data from each receiver channel is multiplexed together for recording onto any of the three available HDDRs.

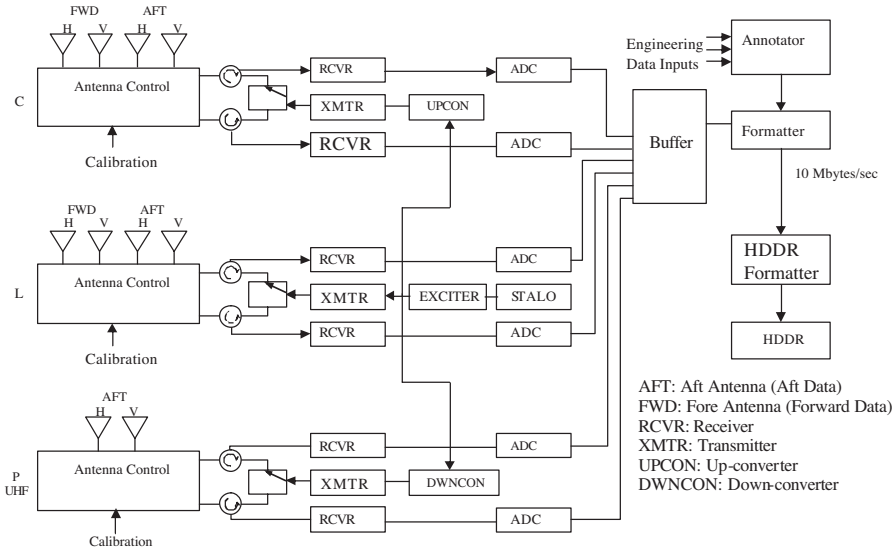

Figure 1.2. NASA/JPL aircraft imaging radar functional diagram.

One of the inexpensive SAR system is the Brigham Young University SAR (YSAR) [12]. Typical SAR system is complex, expensive and difficult to transport but the YSAR is relatively inexpensive and lightweight. This system is to be flown in four or six passenger aircraft at altitudes up to 2000 feet. The simplified block diagram of YSAR is shown in Fig. 1.3. The baseband chirp is generated by a low-cost 200 MHz Arbitrary Waveform Generator (AWG). The transmitter mixes the 100 MHz bandwidth chirp up to 2.1 GHz for transmission. The chirp is transmitted and received with double-sideband (DSB) modulation to reduce the cost. The receiver and local oscillator are used to mix the RF radar return from the antenna to an offset baseband and amplify it so it can be sampled

by the digital system. A standard PC system is used with plug-in cards for analogue-to-digital conversion and digital processing. The computer based system was used for low cost design.

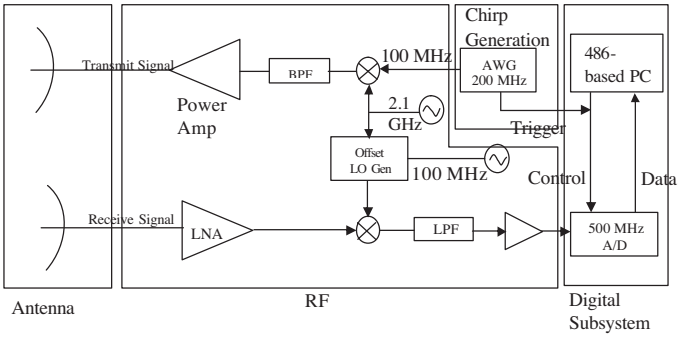

Figure 1.3. YSAR block diagram.

Many other airborne and spaceborne SAR systems are designed for government agency, research institution and private industry. The CCRS C/X- SAR is a multi-frequency, multi-polarisation airborne SAR developed by Canada Centre for Remote Sensing (CCRS) [13]. The system operates in C-band and X-band with both horizontal and vertical polarisation. Sandia National Laboratories has developed a multi-mode Twin-Otter SAR capable of operation on four bands: Ka band, Ku band, X band and VHF/UHF [14]. IFSARE developed by Environmental Research Institute of Michigan (ERIMM) is a X-band single polarisation (HH) interferometry SAR capable of generating up to a 1–3 m height accuracy [15]. C-band, single polarisation (VV) Danish SAR system is developed by Electromagnetics Institute of the Technical University of Demark [16]. The STAR-1 and STAR-2 systems are two fully commercial operational airborne SAR systems operated by Intera Technologies of Calgary [15]. Both are X-band systems. YINSAR is a low cost X-band interferometric SAR developed by Brigham Young University [17]. The European Earth Remote Sensing Satellite (ERS-1) is developed by European Space Agency [18]. It operates in the C-band with a VV polarisation. The Japanese Earth Resources Satellite-1 (JERS-1) is an operational Japanese satellite with SAR sensor operates in L-band with an HH polarisation [19].Shuttle Imaging Synthetic Aperture Radar (SIR) is a cooperative space shuttle experiment between NASA, the German Space Agency (DARA), and the Italian Space Agency (ASI). It equipped with multi-frequency, multi-polarization SAR that operates in the L, C and X-band and provides HH, VV, VH and HV polarization [20]. Most of these systems have been designed and operated for scientific application.

2. PRINCIPLE OF SAR

2.1. Introduction

RADAR is an acronym for **RA**dio **D**etection **A**nd **R**anging. Radar works like a flash camera but at radio frequency. Typical radar system consists of transmitter, switch, antenna, receiver and data recorder. The transmitter generates a high power of electromagnetic wave at radio wavelengths. The switch directed the pulse to antenna and returned echo to receiver. The antenna transmitted the EM pulse towards the area to be imaged and collects returned echoes. The returned signal is converted to digital number by the receiver and the function of the data recorder is to store data values for later processing and display. Fig. 2.1 shows the simply block diagram of a radar system.

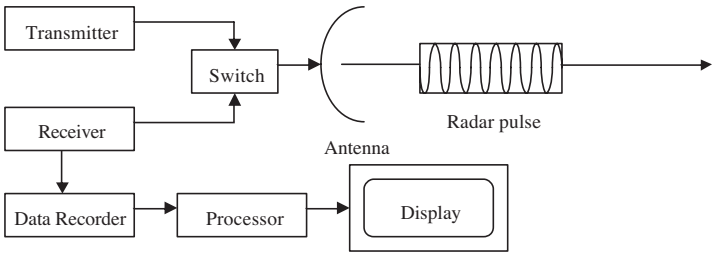

Figure 2.1. Basic block diagram of typical radar system.

The radar platform flies along the track direction at constant velocity. For real array imaging radar, its long antenna produces a fan beam illuminating the ground below. The along track resolution is determined by the beamwidth while the across resolution is determined by the pulse length. The larger the antenna, the finer the detail the radar can resolve.

In SAR, forward motion of actual antenna is used to 'synthesize' a very long antenna. At each position a pulse is transmitted, the return echoes pass through the receiver and recorded in an 'echo store'. The Doppler frequency variation for each point on the ground is unique signature. SAR processing involves matching the Doppler frequency variations and demodulating by adjusting the frequency variation in the return echoes from each point on the ground. Result of this matched filter is a high-resolution image. Figure below shows the synthetic aperture length.

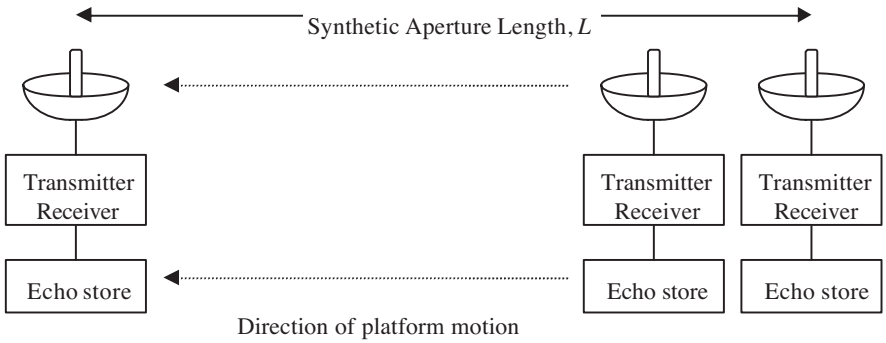

Figure 2.2. Synthetic aperture.

2.2. The Description of an Imaging Radar

The geometry of an imaging radar is shown in Fig. 2.3. The physical aperture of the radar with width W_a and length ℓ generates a RF beam whose angular across track 3 dB beamwidth of antenna and angular along-track 3 dB beamwidth of antenna is θ_V and θ_H respectively. θ_V is determined by the width and length of antenna, and wavelength of transmitted signal (λ). This relation is written as [2],

$$\theta_V = \lambda / W_a \tag{2.1}$$

The antenna is mounted on a platform such as an aircraft that travels along a flight path with velocity v. It illuminates the shaded path (known as footprint) on the ground as the aircraft moves in the direction of flight path. The width of the ground swath is simply given by

$$W_g = \frac{\lambda R}{W_a \cos\theta} \tag{2.2}$$

where θ is the incidence angle (look angle) of the beam, R is the slant range from the antenna to the midpoint of swath.

The RF energy transmitted from antenna has a duration τ_p and is repeated at a given interval, pulse repetition interval (PRI) that can be inverted to obtain the pulse repetition frequency (PRF).

2.2.1. The Resolution of a Real Aperture Radar

Ground resolution is defined as the ability of the system to distinguish between two targets on the ground. Ground range resolution is shown

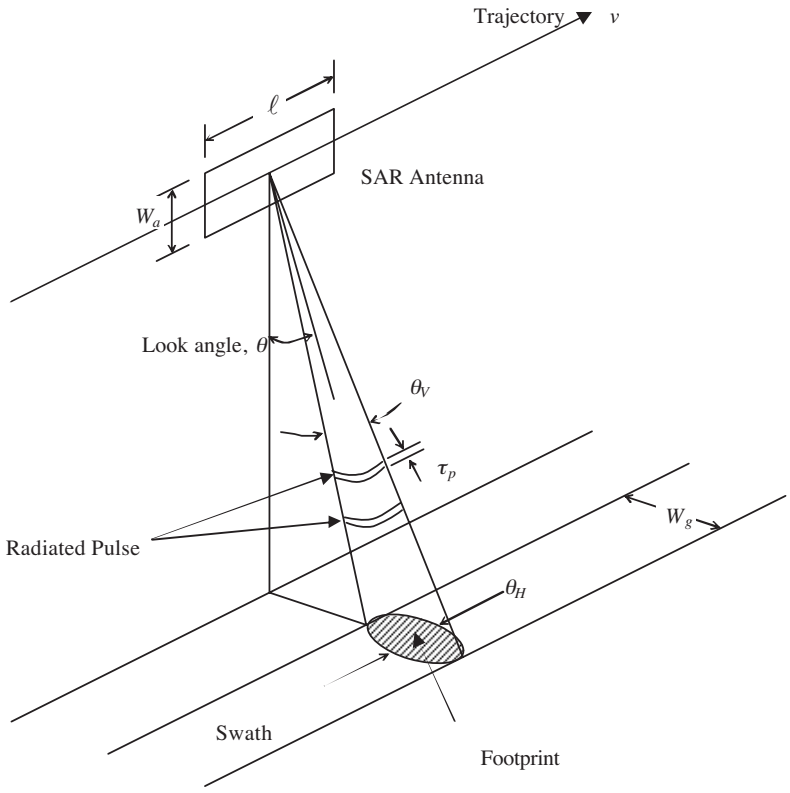

Figure 2.3. The imaging radar geometry.

in Fig. 2.4 as ρ_g. The range resolution of real aperture radar is given as [2],

$$\rho_g = \frac{c\tau_p}{2\sin\theta} \tag{2.3}$$

where τ_p is the pulse length and c is the speed of light. The range resolution is the function of pulse width and look angle but independent of height.

Azimuth resolution is the minimum distance on the ground in the direction parallel to the flight path of the aircraft at which two targets can be separately imaged. Two targets located at same slant range can be resolved only if they are not in the radar beam at the same time. Fig. 2.5 shows the angular spread of the radar beam in the azimuth direction is equal to

$$\theta_H = \lambda/\ell \tag{2.4}$$

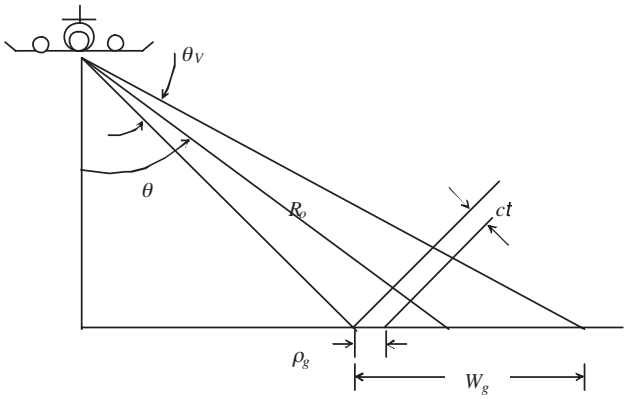

Figure 2.4. Range resolution of a real aperture radar.

Thus, the azimuth resolution can be written as,

$$\rho_a = R\theta_H = \frac{R\lambda}{\ell} \tag{2.5}$$

The azimuth resolution is dependent on aperture length. In order to improve resolution, a longer antenna needs to be employed. The mechanical problems involved in constructing an antenna with a surface precision accurate to within a fraction of wavelength, and the difficulty in maintaining that level of precision in an operational environment, make it difficult to attain values of ℓ/λ greater than a few hundred aperture [2].

2.2.2. Resolution of Synthetic Aperture Radar

SAR is based on the generation of an effective long antenna by signal processing means rather than by the actual use of a long physical antenna. The SAR processing can be achieved by utilising the Doppler effect (frequency shift) of the echo signal [21].

The geometry of SAR is shown in Fig. 2.6. The aircraft is mapping the point, p, whose coordinates are x_o, y_o, 0. The aircraft will fly a synthetic array of length L, centered at $y = 0$ at speed v, parallel to the y-axis and altitude, h_o. The time to fly the array is $T = L/v$. The range from the aircraft to p can be written

$$R = \sqrt{x_o^2 + (y_o - vt)^2 + h_o^2} \tag{2.6}$$

where $-T/2 \leq t \leq T/2$, for $L \ll R$, $R_o = \sqrt{x_o^2 + y_o^2 + h_o^2}$ and

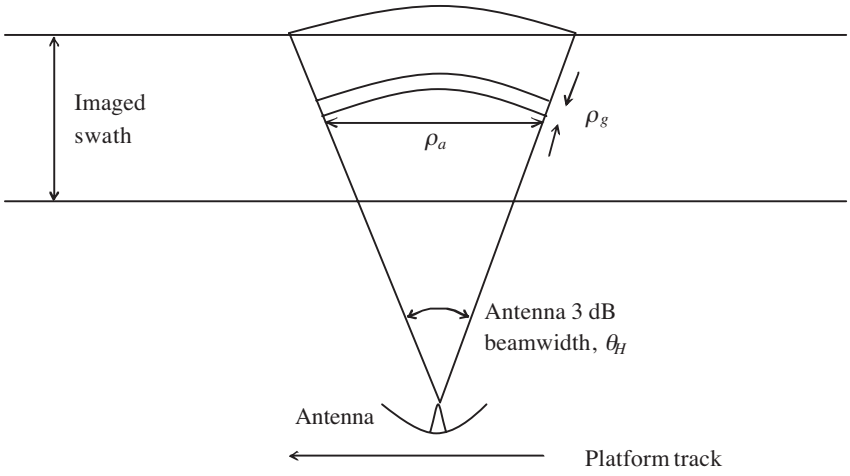

Figure 2.5. Azimuth resolution of a RAR.

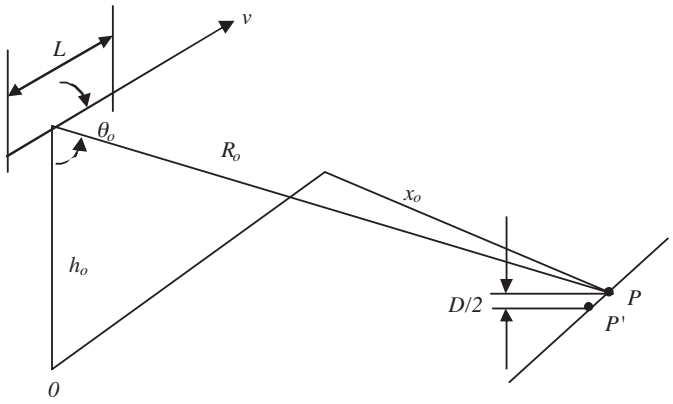

Figure 2.6. Illustration of azimuth resolution of SAR.

$\cos\theta_o = y_o/R_o$, the terms to t^2 in Taylors series expansion for R yield

$$R \cong R_o \left(1 - \frac{vt}{R_o}\cos\theta_o + \frac{v^2t^2}{2R_o^2}\sin^2\theta_o\right) \tag{2.7}$$

Assuming a signal transmitted toward a point scatterer at p as

$$e_1 = A\cos\omega_o t. \tag{2.8}$$

while A is the amplitude and ω_o is the angular frequency, will be

reflected and received at the aircraft with a time delay τ' so that

$$e_2 = KA\cos\omega_o(t-\tau') \tag{2.9}$$

where K is a constant and e_2 is the received signal. The time delay is given as a function of range, R, as $\tau' = 2R/c$. Thus, time delay becomes,

$$\tau' = \frac{2R_o}{c} - \frac{2vt}{c}\cos\theta_o + \frac{v^2t^2}{R_oc}\sin^2\theta_o \tag{2.10}$$

The argument of the received signal with this substitution for τ' is

$$\begin{aligned}\theta(t) &= \omega_o(t-\tau') \\ &= \omega_o t - \frac{2\omega_o R_o}{c} + \frac{2\omega_o vt}{c}\cos\theta_o - \frac{\omega_o v^2t^2}{R_oc}\sin^2\theta_o\end{aligned} \tag{2.11}$$

In terms of wavelength, $\lambda = 2\pi c/\omega_o$,

$$\theta(t) = \omega_o t - \frac{4\pi R_o}{\lambda} + \frac{4\pi}{\lambda}vt\cos\theta_o - \frac{2\pi v^2t^2}{R_o\lambda}\sin^2\theta_o \tag{2.12}$$

Using the usual definition of the instantaneous frequency as

$$f_i = \frac{1}{2\pi}\frac{d\theta(t)}{dt} \tag{2.13}$$

thus, we get

$$f_i = f_o + \frac{2v}{\lambda}\cos\theta_o - \frac{2v^2t}{R_o\lambda}\sin^2\theta_o \tag{2.14}$$

where $f_o = \omega_o/2\pi$. The second term is the doppler shift associated with the squint angle θ_o. The third term represents the change in doppler shift due to the forward motion of the aircraft.

The instantaneous frequency for the two targets, p and p', both at a distance of R_o but separated in azimuth by a distance, $D/2$, will be

$$f_o + \frac{2v}{\lambda}\cos\theta_o \text{ and } f_o + \frac{2v}{\lambda}\cos\theta_o - \frac{vD}{R_o\lambda}\sin\theta_o$$

since the time to fly the distance between them is $t = D\sin\theta_o/2v$ and the observed differential frequency shift Δf_i will be

$$\Delta f_i = \frac{vD}{R_o\lambda}\sin\theta_o \tag{2.15}$$

thus to resolve two targets separated by a distance $D/2$ having a frequency difference of Δf_i, data must be collected for a time $T \cong 1/\Delta f_i$. This results in the synthetic array length,

$$\begin{aligned} L &= vT \\ &= \frac{R_o \lambda}{D \sin \theta_o} \end{aligned} \tag{2.16}$$

Thus from (2.15) and (2.16), we obtain

$$\rho_a = \frac{D}{2} = \frac{\lambda R_o}{2L \sin \theta_o} \tag{2.17}$$

Maximum resolution in the y-direction can be obtained by considering the fact that the antenna illumination coverage on the ground should be greater than the equivalent antenna array length. Using the antenna beamwidth relationships, we get

$$\frac{R_o \lambda}{\ell} > L = \frac{\lambda R}{D \sin \theta_o} \tag{2.18}$$

where ℓ is the actual antenna length and L is the equivalent array length on the ground. Noting that $\rho_a = \frac{D}{2}$, (2.18) for $\theta_o = 90^\circ$ results

$$\rho_a \geq \frac{\ell}{2} \tag{2.19}$$

The best y-direction resolution obtainable is equal to one half of the actual antenna length ℓ, independent of range, wavelength and pointing. This implied that smaller antenna can obtain better resolution.

2.2.3. SAR Processing

The main goal of SAR data processing is the determination of the range and azimuth coordinates of the targets lying in the strip-map. The SAR data space is a conceptual collection of SAR data arranged by range line (1, 2, 3, 4, ...) with the first data point from each range line at the top and the last data from each range line at the bottom [22]. A range line is a recording of all the reflections from a single transmitted chirp pulse. This data space is shown in Fig. 2.7.

Generally there are two approaches for SAR processing, namely Two-dimension Algorithm and Range Doppler Processing Algorithm. Two-dimension Algorithm processes the range and azimuth data simultaneous whereas the Range Doppler Processing algorithm

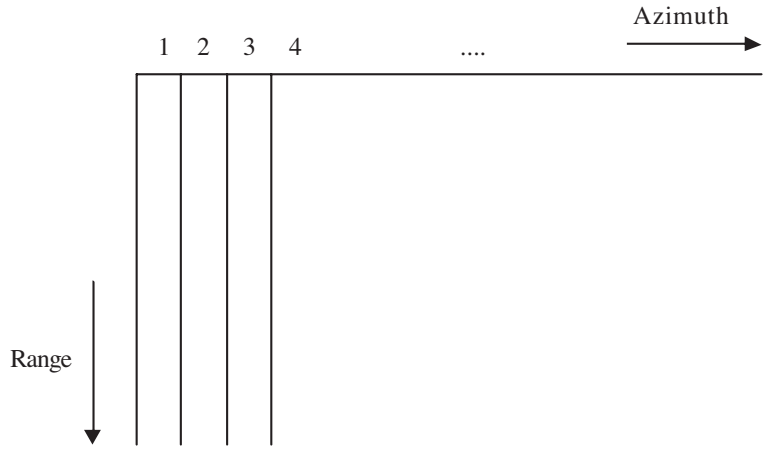

Figure 2.7. Two-dimensional SAR data space.

implements range compression processing followed by azimuth compression processing. However, Two-dimension Algorithm proposed by Alan Di Cenzo [23] required larger memory and computational power.

The most common algorithm employed in most the SAR processing system is the Range Doppler Processing algorithm. It is a two-dimensional correlating procedure. The two dimensions of the correlation processing are realised as two one-dimensional matched filter operations namely range compression and azimuth compression. The first matched filtering operates on the single pulse radar returns (detail described in Section 2.3) and the second matched filtering operation operates on the Doppler signal. Fig. 2.8 shows the basic concept of the SAR processing.

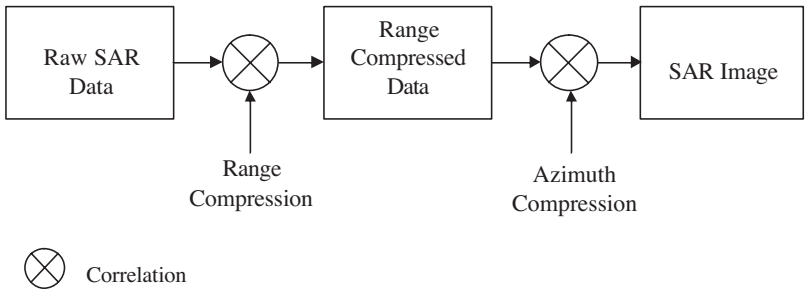

Figure 2.8. Range-doppler processing.

2.3. Matched Filter and Pulse Compression

The matched filter and pulse compression concepts are the basic of SAR processing algorithms [2]. The matched filter is a filter whose impulse response, or transfer function is determined by a certain signal, in a way that will result in the maximum attainable signal to noise ratio. Pulse compression involves using a matched filter to compress the energy in a signal into a relative narrow pulse.

2.3.1. Basic Properties of Matched Filter

A matched filter is designed to maximise the response of a linear system to particular known signal. Fig. 2.9 shows the basic block diagram of a matched filter radar system. The transmitted waveform is generated by a signal generator designated as $s(t)$. The signal output from $s(t)$ is amplified, fed to antenna, radiated, reflected from a target and return to receiver. The output of receiver is fed into the matched filter after suitable amplification. The matched filter impulse response, $h(t)$, is simply a scaled, time reversed and delayed form of the input signal. The shape of the impulse response is related to the signal and therefore matched to the input. The matched filter has the property of being able to detect the signal even in the presence of noise. It yields a higher output peak signal to mean noise power ratio for the input than for any other signal shape with the same energy content.

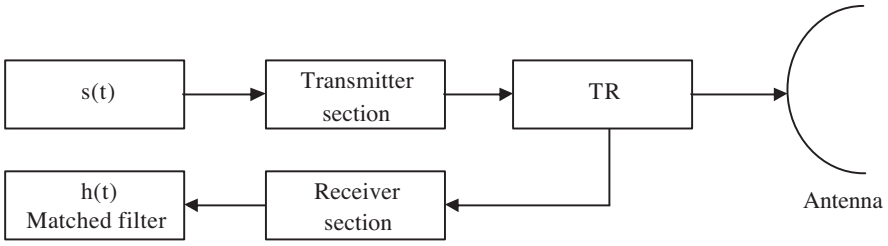

Figure 2.9. Basic matched filter radar system.

Assuming return signal is a replica of transmitted signal with a time delay t_o. The filter is matched to $s(t)$ and has an impulse response of

$$h(t) = Ks(t_o - t) \tag{2.20}$$

where t_o is a delay and K is a constant. The Fourier Transform (FT) of the impulse response of $h(t)$ is known as the transfer function of the

matched filter, *H(jw)* and can be written as

$$H(jw) = FT\{h(t)\} \tag{2.21}$$

$$H(jw) = \int_{-\infty}^{\infty} h(t)e^{-jwt}dt \tag{2.21}$$

Substituting $h(t)$ from Equation (2.20),

$$H(jw) = K\int_{-\infty}^{\infty} s(t_o - t)e^{-jwt}dt \tag{2.23}$$

By changing the time variable as, $\tau = t_o - t$, (2.23) is given as,

$$H(jw) = -K\int_{-\infty}^{\infty} s(\tau)e^{jw\tau}d\tau \tag{2.24}$$

The FT of $s(t)$ is written as,

$$S(jw) = \int_{-\infty}^{\infty} s(\tau)e^{-jwt}dt \tag{2.25}$$

The complex conjugate of $S(jw)$, $S^*(jw)$ is given as

$$S^*(jw) = S(-jw) \tag{2.26}$$

From the equations above, $H(jw)$ can be written as,

$$H(jw) = -Ke^{-jwt_o}S^*(jw) \tag{2.27}$$

The transfer function of the matched filter obtained is the complex conjugate of the spectrum of the signal to which it is matched. Hence, the impulse response $h(t)$ of the matched filter is a scaled, time reversed and delayed version of the desired signal.

The output of a matched filter when a signal, $s(t)$ is impressed at the input can be computed with the expressions derived for the transfer function. In the time domain, the output can be obtained either by the convolution integral or the cross correlation integral. For the convolution integral, let $y(t)$ be the output of the matched filter. The output, $y(t)$, is then given by:

$$y(t) = h(t) * s(t) = \int_{-\infty}^{\infty} h(t-u)s(u)du \tag{2.28}$$

Since the input signal lasts for a short duration, the output is given by:

$$y(t) = \int_{-\tau/2}^{\tau/2} h(t-u)s(u)du \tag{2.29}$$

If the cross correlation integral is considered, the output is given by the cross correlation of $h(-t) \otimes s(t)$ as:

$$y(t) = h(-t) \otimes s(t) = \int_{-\tau/2}^{\tau/2} h(-u)s(t+u)du \tag{2.30}$$

Changing the time variable as $-u = t - v$, (2.30) is given as

$$y(t) = h(-t) \otimes s(t) = \int_{t-\tau/2}^{t+\tau/2} h(t-v)s(v)dv \tag{2.31}$$

or,

$$y(t) = h(-t) \otimes s(t) = \int_{-\tau/2}^{\tau/2} h(t-v)s(v)dv \tag{2.32}$$

Equations (2.29) and (2.32) are essentially equivalent, except for the sign reversal in the impulse response function for the cross correlation integral. Thus $y(t)$ is,

$$y(t) = h(t) * s(t) = h(-t) \otimes s(t) = \int_{-\tau/2}^{\tau/2} h(t)s(\tau - t)dt \tag{2.33}$$

In the frequency domain, the output, $Y(jw)$ can be obtained from the transfer function as follows:

$$Y(jw) = H(jw)S(jw) = -Ke^{-jwt_o}S(jw)S^*(jw) \tag{2.34}$$

The output, $y(t)$, is obtained by taking the Inverse Fourier Transform (IFT) as shown below,

$$y(t) = IFT\{Y(jw)\} \tag{2.35}$$

2.3.2. Pulse Compression

Range resolution for a given radar can be significantly improved by using short pulse. Unfortunately utilising short pulse decreases the average power, which degrades radar signal detectability and

measurement precision. Since the average transmitted power is directly linked to the receiver Signal to Noise Ratio (SNR), it is desired to increase the pulse width while simultaneously maintaining adequate range resolution. This can be accomplished by using pulse compression technique. Pulse compression allows achieving the average transmitted power of a relatively long pulse, while obtaining the range resolution corresponding to a short pulse [24]. The increased detection capability of a long-pulse radar system is achieved while retaining the range-resolution capability of a narrow-pulse system.

The distinguishing feature of a pulse compression waveform is a time-bandwidth product that is larger than unity. For pulse type waveform, one of the most attractive ways of increasing the time bandwidth product is to use continuous phase modulation. This can be achieved by implementing the phase modulation or frequency modulation to the transmitted signal. There are three popular types of pulse compression waveform, the linear frequency modulation (LFM) or chirp, non-linear frequency modulation and phase coded. The LFM, or chirp waveform has achieved pre-eminence for a variety of reasons — They are easy to generate, they provide both good range resolution and they are easy to process. Besides that many diverse techniques and devices have been developed to provide the pulse compression processing required by these signals. On the other hand, the disadvantages of non-LFM and phase coded waveform included greater system complexity; waveform difficult to generate; and limited development of generation devices.

2.3.3. LFM Waveform

The LFM waveform is the most widely discussed pulse compression waveform in the literature and most extensively used in practice. The utility of chirp waveform in imaging radar comes about because the duration of this signal can be long compared to that of CW burst pulse and yet the result is the same effective bandwidth. LFM signals have the characteristic that the instantaneous frequency increase (or decreases) linearly over the duration of the signal. Thus the chirp waveform can be described by the $Re\{s(t)\}$ with

$$s(t) = \exp\left[j2\pi\left(f_c t + kt^2/2\right)\right] \tag{2.36}$$

where $s(t)$ is 0 everywhere outside of the interval $-\tau/2 \leq t \leq \tau/2$. f_c is the carrier frequency of transmitted waveform, k is the chirp rate of the waveform. The bandwidth of the signal is given by

$$B = k\tau \tag{2.37}$$

The instantaneous frequency, $f(t)$, is given as,

$$f(t) = \frac{1}{2\pi}\frac{d\phi(t)}{dt} = f_c + kt \tag{2.38}$$

The frequency time characteristics of transmitted signal are given in Fig. 2.10. The transmitted pulse duration is τ and frequency modulated from f_1 to f_2. The bandwidth of the signal is $B = f_2 - f_1 = k\tau$. The effect of frequency modulation on the transmitted sinusoidal signal is shown in Fig. 2.10(c). Although the LFM signal has a duration of τ, it can behave like a pulse with duration equivalent to the inverse of its bandwidth, i.e., $\tau_{eq} = 1/B$. The signal processing that allows this to happen is known as pulse compression. The amount of this compression is given by $\tau/\tau_{eq} = \tau B = D$, which is the time bandwidth product of the waveform.

The linear FM chirp exhibits the interesting property of possessing

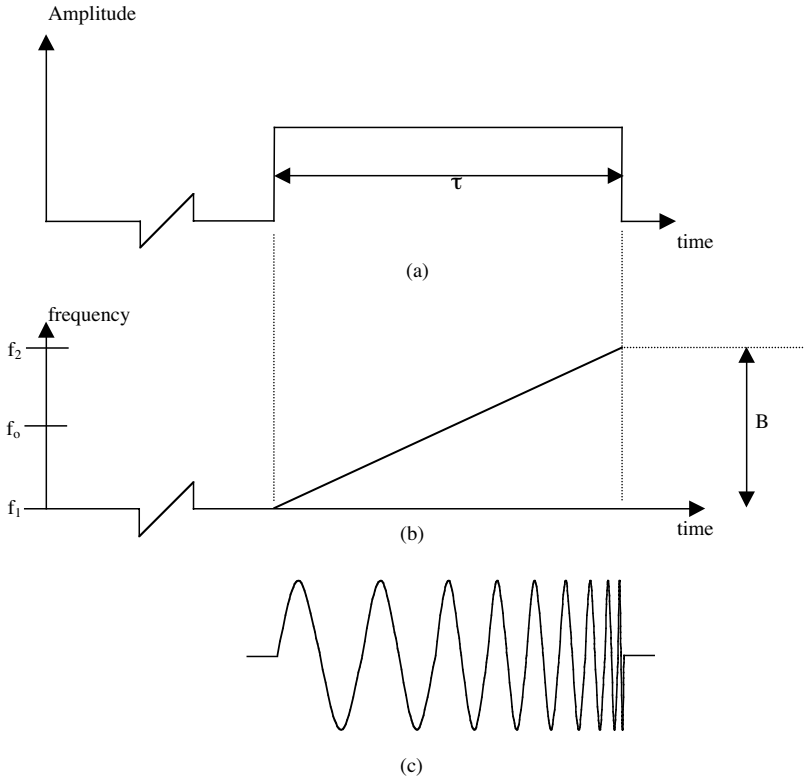

Figure 2.10. Linear FM waveform.

very large time-bandwidth products [25]. To demonstrate the large time bandwidth product aspect of dispersed waveforms, simulation of a linear FM chirp waveform and a continuous wave (CW) burst that have the same bandwidth have been done. The duration of the LFM, however is 500 times greater than of the effective duration of the CW burst. Fig. 2.11 shows the discrete Fourier Transform of the two waveforms. The transform of the chirp is essentially flat over its range of frequencies.

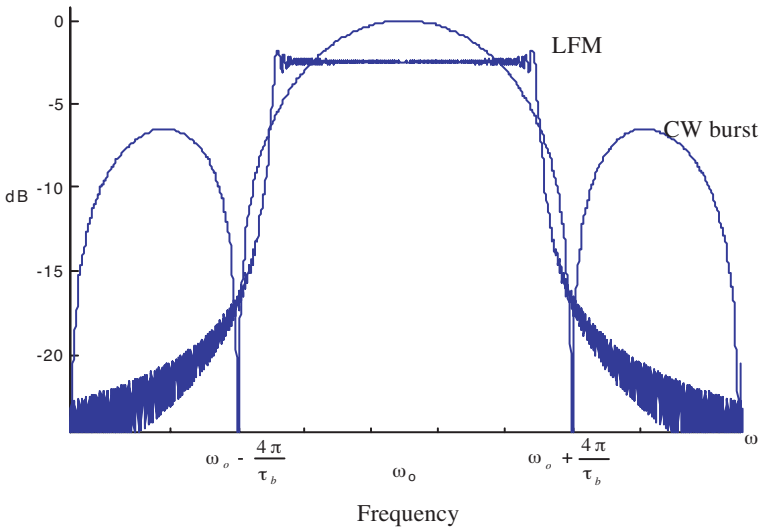

Figure 2.11. Fourier transform magnitude of CW burst and LFM waveforms.

The generation of LFM waveform can be divided into two general categories, passive or active generation. Passive generation involves exciting a device or network with a short pulse to produce a time-expanded coded waveform. This including electrical devices that use the dispersive characteristics of an electrical network and ultrasonic devices in which an electrical signal is converted into a sonic wave. Active generation involves generating the waveform by phase or frequency modulation of a carrier without the occurrence of an actual expansion. Some common techniques in active generation include voltage controlled oscillator, delay line generator and recent trend of LFM signal generation using digital approach such as Direct Digital Synthesizer (DDS), Field-Programmable Gate Array (FPGA), etc. [26]. Active generation can provided greater waveform flexibility since bandwidth and pulse width can be varied easily. Furthermore,

the waveform is simpler to generate.

Processing of LFM waveform can also be divided into two general classes, namely passive and active processing. Passive processing involves the used of a compression network that is conjugate of expansion network and is a matched-filtering approach. Active processing involves mixing delayed replicas of the transmitted signal with the received signal and is a correlation processing approach. The active processing reduces the complexity of system design and hardware implementation.

2.3.4. Matched Filter Response for LFM Waveform

The transmitted signal is given by (2.36)

$$\begin{aligned} s(t) &= \cos\left[j2\pi\left(f_c t + kt^2/2\right)\right], \quad -\tau/2 \le t \le \tau/2 \\ &= 0, \qquad\qquad\qquad\qquad\quad \text{elsewhere} \end{aligned}$$

The matched filter has an impulse response, $h(t)$, that is time inverse of the signal at receiver input as given below

$$h(t) = K\cos\left\{2\pi\left(f_c t - \frac{1}{2}kt^2\right)\right\}, \quad -\tau/2 \quad \le t \le \tau/2 \qquad (2.39)$$

where K is factor that result in unity gain. Since the echo from the target at time t_o is delayed replica of the transmitted signal, the return signal is given as

$$s(t_o) = \cos\left\{2\pi\left(f_c + f_d t_o + \frac{1}{2}kt_o^2\right)\right\} \qquad (2.40)$$

where $s(t_o)$ represent the return echo from target and f_d is the shifted in frequency cause by the Doppler effect.

From above equation, the matched filter characteristics of (2.39), and the convolution integral of (2.33), the general output of matched filter can be written as

$$\begin{aligned} g(t_o,\omega_d) \;=\; K\int_{-\tau/2}^{\tau/2} \cos\left\{(\omega_c+\omega_d)t + \frac{1}{2}k(2\pi)t^2\right\}\cos\left\{\omega_c(t_o-t)\right. \\ \left. +\frac{1}{2}k(2\pi)(t_o-t)^2\right\}dt \end{aligned} \qquad (2.41)$$

where ω_c=$2\pi f_c$ and ω_d=$2\pi f_d$.

The closed form solution of above equation can be obtained through a considerable amount of trigonometric and algebraic

manipulation. The result of this calculation is given as,

$$g(t_o, \omega_d) = G\cos\left\{\left(\omega_o + \frac{\omega_d}{2}\right)t_o\right\}\frac{\sin\left\{\frac{\omega_d+2\pi k t_o}{2}(\tau - |t_o|)\right\}}{\frac{\omega_d+2\pi k t_o}{2}}, \quad -\tau/2 \le t \le \tau/2 \tag{2.42}$$

where $|t_o|$ is the absolute value of t_o. Note that the above equation is in the form of $\frac{\sin X}{X}$.

2.3.5. Range Resolution of LFM Waveform

From (2.36), the linear FM transmitted pulse can be written as,

$$s(t) = E_o\cos\left[j2\pi\left(f_c t + kt^2\right)\right], \quad -\tau/2 \le t \le \tau/2 \tag{2.43}$$

where E_o is the signal amplitude, f_c is the signal carrier frequency and k is the chirp rate. The frequency of the signal sweeps through a band $-\frac{k\tau}{2} \le (f - f_c) \le \frac{k\tau}{2}$ so that the bandwidth of the signal, B is equal to the product of the chirp slope and the pulse duration.

The return echo from the target is down converted by shifting the spectrum of return signal according to the reference signal carrier frequency and filtering the result to recover only the frequency band centred about baseband frequency with bandwidth B. Both in-phase and quadrature-phase components of the signal can be extracted and this operation is known as "I, Q detection". The output of the filtering process can be written as,

$$g(t - t_o) = E_o^2 B sinc\pi B(t - t_o) \tag{2.44}$$

where t_o is the delay of he return from the point target and time-width of $g(t)$ is $1/B$. Substituting $1/B$ for τ_p in Equation (2.3) gives,

$$\rho_g = \frac{c}{2B\sin\theta} \tag{2.45}$$

The larger bandwidth in linear FM, the better range resolution can be achieved.

2.3.6. Stretch Processor

Active processing can be basically divided into two techniques [24]. The first technique is known as "correlation processing" which is normally used for narrow and medium band radar operation. The second technique is called "stretch processing" or "deramp compression

processing" and is normally used to process high bandwidth LFM waveform. The stretch processing technique is employed since it is much easier to implement. Others advantages include reduced signal bandwidth, dynamic range increase due to signal compression, and the baseband frequency offset is directly proportional to the target range. Beside that, the correlation processing employed the amplitude modulating that introduces extra burdens on the transmitter hence increase the hardware complexity.

The block diagram for a stretch processing receiver is shown in Fig. 2.12. The stretch processing consists of the following steps: first of all the received signals are mixed with a reference signal from the local oscillator (LO). Hence, active-correlation multiplication is conducted at RF followed by lowpass filtering to extract the difference frequency terms. The signal is split into I and Q components and digitised for further processing. The return from each range bin within the selected range gate thus corresponding to a pulsed sinusoid at the output of the active difference mixer. The later the return, the higher the residual frequency. Pulse compression is completed by performing a spectral analysis of the difference-frequency output to transform the pulse tones into corresponding frequency resolution cells. Spectral analysis is performed by digitising the difference frequency output and processing it through an FFT.

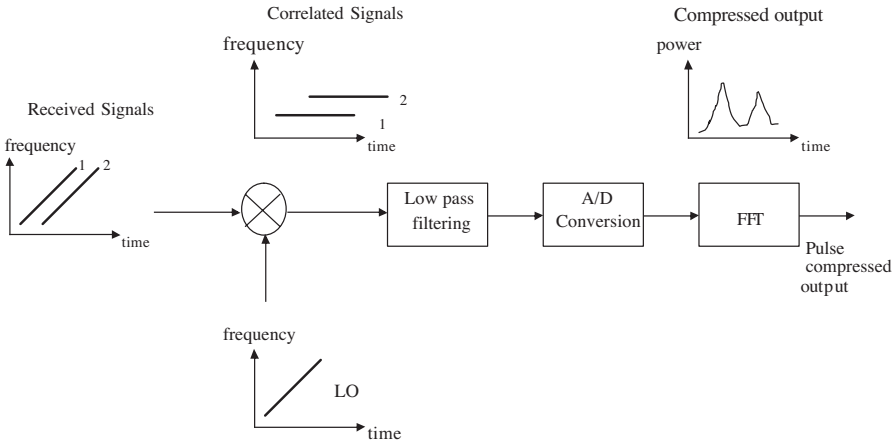

Figure 2.12. Stretch pulse compression.

Figure 2.13 shows the frequency against time in deramp compression processing. The TX, REF and RX represent the transmitted signal, the reference signal, and the received signal from a point targets respectively. The reference signal is generated such

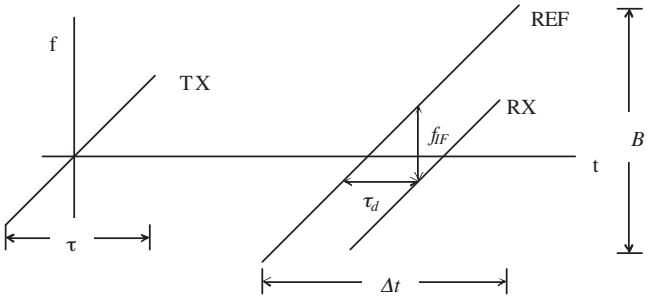

Figure 2.13. Deramp range compression.

that its length Δt is the timewidth of the slant range swath over which returns are expected. The frequency of the reference signal is linearly swept over a RF bandwidth, B. The received signal is a replica of transmitted signal with a time delay τ_d. From the geometry of Fig. 2.13, the IF frequency, f_{IF} can be written as,

$$\frac{f_{IF}}{\tau_d} = \frac{B}{\Delta t}$$

or

$$f_{IF} = \frac{B}{\Delta t}\tau_d \tag{2.46}$$

2.4. The SAR Radar Equation

The radar equation for a monostatic radar system can be written as

$$P_r = \frac{P_t G^2 \lambda^2 \sigma}{(4\pi)^3 R^4} \tag{2.47}$$

where

P_r=power received at the antenna
P_t=power radiated by the antenna
G=antenna gain
R=distance from radar to the target
λ=operating wavelength
σ=radar target cross section

Signals received by radar are usually contaminated by noise due to random modulations of the radar pulse during atmospheric propagation, or due to fluctuations in the receiving circuits. The signal

to noise ratio (SNR) is defined as:

$$SNR = \frac{S}{N_o} = \frac{P_t G^2 \lambda^2 \sigma}{(4\pi)^3 R^4 N_o} \tag{2.48}$$

The receiver noise can originate within the receiver itself or it may enter the receiver through the receiving antenna. The thermal noise of the receiver can be written as

$$\text{Thermal noise} = kTB_n \tag{2.49}$$

where k is the Boltzmann's constant and is equal to 1.38×10^{-23} joules per degree, T is effective noise temperature, and the equivalent noise bandwidth B_n, in HZ. The total receiver noise is given by

$$N_o = FkTB_n \tag{2.50}$$

where F represents the experimentally determine constant called noise figure. For a target seen against receiver noise, the SNR per pulse is then:

$$SNR = \frac{P_t G^2 \lambda^2 \sigma}{(4\pi)^3 R^4 k T_o B_n F} \tag{2.51}$$

Hence the SNR after SAR processing, for a point target of cross section σ at range R is:

$$SNR = \frac{P_t G^2 \lambda^2 \sigma n}{(4\pi)^3 R^4 N_o} \tag{2.52}$$

This improvement in SNR by a factor of n after coherent integration of synthetic aperture length. The number of elements, n, which comprise the synthetic aperture is:

$$n = T_s . f_r \tag{2.53}$$

where T_s is the time over which the aperture is formed and f_r is the pulse repetition frequency. T_s is related to synthetic aperture length, L via:

$$T_s = \frac{L}{v} = \frac{\lambda R}{2 v \rho_a \sin\theta_o} \tag{2.54}$$

where ρ_a represent azimuth resolution, f_r represent pulse repetition frequency, θ is the look angle of the antenna beam and v is the velocity

of platform. The total number of pulse integrated over coherent integration time will be

$$n = \frac{f_r R\lambda}{2\rho_a v \sin\theta_o} \tag{2.55}$$

Thus the final form of the SAR radar equation for a point target is:

$$SNR = \frac{P_t G^2 \lambda_r^3}{(4\pi)^3 R^3 N_o 2\rho_a v \sin\theta_o} \tag{2.56}$$

For a point target in a SAR image, the SNR improves with finer azimuth resolution.

For a distributed target, The radar target cross section can be expressed in terms of azimuth and range resolution cell, ρ_a and ρ_g as,

$$\sigma = \rho_a \rho_g \sigma_o \tag{2.57}$$

where σ_o is the backscattering coefficient. From (2.56) and (2.57), the SAR radar equation become,

$$SNR = \frac{P_t G^2 \lambda^3 \sigma_o \rho_g f_r}{(4\pi)^3 R^3 N_o 2v \sin\theta_o} \tag{2.58}$$

Assuming an initial uncompressed pulse duration of τ_i and a compressed pulse duration of τ_c, the pulse compression ratio D can be written as

$$D = \frac{\tau_i}{\tau_c} \tag{2.59}$$

Finally, utilising the relation for the average power $\overline{P}$ as a function of peak power P of (2.52), we obtain

$$\overline{P} = P\tau_i f_r \quad \text{or} \quad P = \frac{\overline{P}}{\tau_i f_i} \tag{2.60}$$

Using relation (2.58) through (2.59) in (2.60), we get

$$SNR = \left(\frac{\overline{P}}{\tau_i f_r}\right)(G^2\lambda^2)(\rho_a \rho_r \sigma_o)\left(\frac{\tau_i}{\tau_c}\right)\left(\frac{f_r R\lambda}{2\rho_a v}\right)/(4\pi)^3 R^4 (FkTB_n)\sin\theta_o \tag{2.61}$$

where SNR represent the total signal to noise ratio. Simplified the (2.61), we obtain

$$SNR = \frac{\overline{P} G^2 \lambda^3 \rho_g \sigma_o}{(2v)(4\pi)^3 kTFR^3 \sin\theta_o} \tag{2.62}$$

Rearrange of above equation will result

$$\overline{P} = \left(\frac{(4\pi)^3 R^3 kTF}{G^2\lambda^2\sigma_o\rho_g}\right)\left(\frac{2v}{\lambda}\right)(SNR)\sin\theta_o \tag{2.63}$$

For strip-mode SAR, the squint angle, $\theta_o = 90^\circ$, therefore (2.63) can be written as

$$\overline{P} = \left(\frac{(4\pi)^3 R^3 kTF}{G^2\lambda^2\sigma_o\rho_g}\right)\left(\frac{2v}{\lambda}\right)(SNR) \tag{2.64}$$

Equation (2.64) leads to the conclusion that in SAR system the SNR is: 1) inversely proportional to the third power of range; 2) independent of azimuth resolution; 3) function of the ground range resolution; 4) inversely proportional to the velocity; and 5) proportional to the third power of wavelength. From (2.62), increased resolution in range direction, i.e., smaller ρ_g, will require increased transmitted power. In a number of synthetic array radar this is achieved by pulse compression technique.

2.5. In Phase and Quadrature (IQ) Sampling

The sampling rate of the analogue signal can be reduced by separating the signal into two waveforms, and sampling each channel at its Nyquist rate. This is based on the principle that a signal can be expressed in terms of two waveforms called quadrature functions [22]. The concept of IQ sampling is illustrated in Fig. 2.14.

An input waveform $x(t)$ with a bandwidth f_w is multiple by a cosine in one channel and a phase shifted cosine in the other channel. The second cosine is phased shifted by 90° (or one quadrant). The cosine term is assigned to the real axis and is known as in-phase term. The second channel is shifted by one quadrant and is commonly called the quadrature term. $X(f)$, $Y_i(f)$ and $Y_q(f)$ are the Fourier transform of $x(t)$, $y_i(t)$ and $y_q(t)$ respectively.

The multiplication in the time domain is equivalent to the convolution in the frequency domain. This results each of two quadrature functions occupies only one half the bandwidth of original signal. Therefore it is possible to sample each quadrature signal at one half sampling rate required to sampled the original signal.

3. SAR SYSTEM DESIGN CONSIDERATION

The parameters of a SAR system depend on the primary goal of the project and are determined cooperatively by the system engineer and

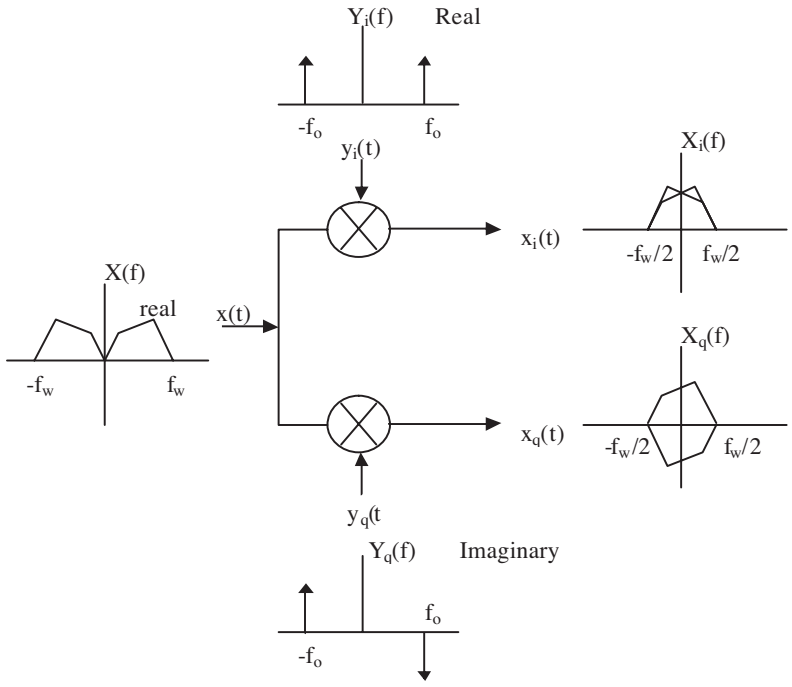

Figure 2.14. Quadrature sampling.

the customer. Different system-level objective will lead to different radar configuration. Some of the parameters are selected by the radar engineers in a logical manner whenever possible, using some suitable criterion such as minimizing total cost, minimizing development time, or maximizing likelihood of success. When the system is too complex for logical selection of the radar parameters, or when the criteria are not too clear and the inputs needed for analytical system design are uncertain, the system engineer must make decisions based on his experience and engineering judgement. Some of the SAR system design considerations include:

1) Operating Frequency

For remote sensing applications, frequency range from 1 to 30 GHz is normally used. In the 1–10 GHz range, the transmissivity through air approaches 100%. Thus, a SAR operating in this frequency range is always able to image the earth's surface independent of the cloud cover or precipitation. As the radar frequency increases, the transmission attenuation increases. At 22 GHz there is a water vapour absorption

band that reduces transmission to about 85%.

2) Modulations

In SAR system, there are basically three types of widely used modulation schemes: pulse, LFM or chirp and phase coded. Pulse system is used in older generation radar. Modern radar uses LFM waveform to increase range resolution when long pulses are required to get reasonable signal to noise ratio. The same average transmitting power as in a pulse system can be achieved with lower peak amplitude. The LFM configuration is employed in this project since it gives better sensitivity without sacrificing range resolution and ease of implementation. The lower peak power allows for the use of commercially available microwave components that have moderate peak power handling capability. Phase coded modulation is not prefer due to it's difficulty to generate. Phase coded modulation normally used for long duration waveforms and when jamming may be a problem.

3) Mode of Operation

Available data acquisition mode includes strip-mapping, squint mode, spotlight mode, ScanSAR, interferometry and polarimetric SAR. Spotlight mode SAR provides high-resolution image but involves complex hardware and processing algorithm. Squint mode SAR is used to image while maneuvering. It usually employed in military aircraft. ScanSAR is normally used in spaceborne SAR in order to increase the swath width. It requires powerful computation hardware. Polarimetric system capable of measuring scattering matrix S of target whereas interferometry SAR is the latest technology developed with capability of measuring terrain high and constructing three dimensional image. Hardware design of interferometry and polarimetric SAR is more complicated.

4) Polarisation

Conventional SAR system employed single polarisation such as VV or HH to acquire information from earth. For remote sensing of earth terrain such as oil palm plantation or tropical forest, single polarisation is sufficient. A device which measures the full polarisation response of the scattered wave is called a polarimeter. Polarimetric systems differ from conventional system in that they are capable of measuring the complete scattering matrix of the remotely sensed media. By having the knowledge of the complete scattering matrix, it is possible to calculate the backscattered signal for any given combination of the transmitting and receiving antennas. This process is called the

polarisation synthesis, which is an important technique used in terrain classification [27–29].

5) Dynamic Range of Backscattering Coefficient σ°

The required system sensitivity is determined based on the various categories of earth terrain to be mapped such as man made target, ocean, sea-ice, forest, natural vegetation and agriculture, geological targets, mountain, land and sea boundary. From the open literatures, the typical value of σ° falls in the range of +20 dB to −40 dB [30, 31]. For vegetation the typical value of σ° vary from +0 dB to −20 dB.

6) Operating Platform

Basically SAR systems can be separated into two groups: airborne system operating on variety of aircraft and spaceborne system operating on satellite or space shuttle platforms. Spaceborne SARs have smaller range of incidence angle and larger swath width, but high data rate is a problem. Whereas airborne SARs illuminated smaller footprint on the earth and the data rate is much lower.

7) Spatial Resolution

Typical resolution of airborne SAR range from 1 m to 20 m [15]. It depends mostly on the application requirements. Table below shows some science applications vs. resolutions of airborne SAR.

Table 3.1. Science applications vs. resolution requirement.

Discipline	**Resolution**
Vegetation classification	5–20 m
Soil Moisture and Salinity	5–50 m
Hydrology	5–20 m
Oceanography	50–200 m
Archaeology	2–20 m

8) Swath Width and Range of Incident Angle to be covered

From the open literature, the swath width for airborne SAR range from 5 km to 60 km depends on altitude of operating platform and incidence angle. From the open literatures, the incident angle from 0°–80° is utilised by present airborne SARs. The backscattering coefficient of nature targets such as soil, grass and vegetable are maintained almost constant over the incident angle of 40° to 60° [1, 32].

9) Pulse Repetition Frequency (PRF)

The upper limit of PRF is attained from a consideration of the maximum mapping range and the fact that the return pulse from this range should come within the interpulse period [21]. In order to adequately sample the Doppler bandwidth, the radar must be pulse with a PRF greater or equal to this bandwidth. Combination of lower and upper limit, we obtained

$$\frac{2v}{\ell} \leq PRF \leq \frac{c}{2R_{far}}$$

where R_{far} is the far range from the airborne platform.

10) Antenna

Yagi, slotted-waveguide, horn, dish, and microstrip antennas have found some applications in SAR one time or another. Table 3.2 shows a summary of some selected SAR systems. Yagi is suited for lower frequency applications, while dish is suited for very high frequency application. Modern civilian SAR system generally operate in L- C- and X-band, where slotted-waveguide and microstrip antennas provide the best performance.

4. DESIGN PARAMETERS

The design consideration in Section 3 can be used as the basic guideline to select the suitable microwave system parameters. Basically, the system hardware consists of (i) the microwave components such as antenna, oscillator, mixer, power amplifier and circulator, and (ii) the low frequency electronics components such as integrated circuits, resistors and capacitors. The design of the microwave subsystem is generally more difficult to handle. Therefore, the microwave subsystem was given more attention in the initial stage of the design. The low frequency sections were carefully designed to match the microwave's specifications.

Subsystem level design determines the requirements of SAR subsystem. The requirements will be based on the design parameters decided in Section 3. The radar subsystem can be functionally divided into three assemblies: (i) Transmitter; (ii) Receiver; and (iii) antenna. Each of these assemblies can be further divided into subassemblies and components. Fig. 4.1 shows the block diagram of the SAR system. The transmitter generated the required signal and transmitted via an antenna. Part of the energy is intercepted by the target and reflected back to the receiving antenna. The received echoes

Table 3.2. Comparison of antenna parameters between SAR system.

Name of the project	Frequency of operation	Antenna type	Gain	Beamwidth (degree)	
				Az	Ele
NASA AIRSAR	P-band	All Microstrip	14 dBi	19	38
	L-band		18 dBi	8	44
	C-band		24 dBi	2.5	50
DLR E-SAR	P-band	Microstrip	12 dBi	30	60
	L-band	Microstrip	17 dBi	18	35
	S-band	Microstrip	n.a.	20	35
	C-band	Microstrip	17 dBi	19	33
	X-band	Horn	17.5 dBi	17	30
CCRS C/X SAR	C-band	All Horn	26 dBi	3.3	25
	X-band		28.5 dBi	1.4	26
NASDA X/L-band SAR	L-band	Microstrip	18 dBi	2.3	40
	X-band	Waveguide-slot	26.5 dBi	2.3	40
DCRS EMISAR	L-band	All Microstrip	17.1 dBi	10	42
	C-band		26 dBi	2.4	31
Lynx	Ku-band	Horn-fed dish	n.a.	3.2	7
PHARUS C-band SAR	C-band	Microstrip	n.a.	2.3	24

are amplified and down-converted to lower frequency in the receiver. Further amplification and filtering process is done by IF section of the receiver. Finally the IF signals are digitised and stored in high-density digital recorder for future analysis.

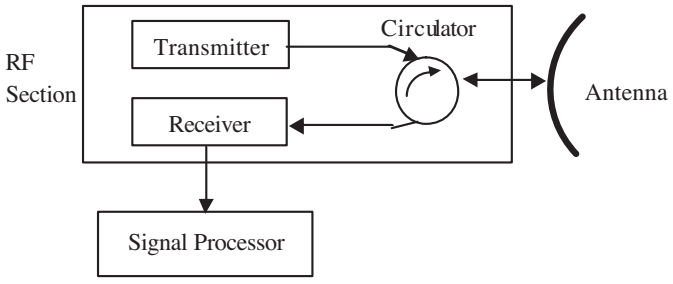

Figure 4.1. System block diagram.

5. CONCLUSION

The Synthetic Aperture Radar (SAR) is an all-weather imaging tool that achieves fine along-track resolution by taking the advantage of radar motion to synthesize a large antenna aperture. SAR technology has provided terrain structural information to geologists for mineral exploration, oil spill boundaries on water to environmentalists, sea state and ice hazard maps to navigators, and reconnaissance and targeting information to military operations. There are many other applications or potential applications. This paper serves as a basic study of SAR. The principle of SAR is described and basic SAR signal processing concept is discussed. Besides the overview of design consideration for SAR system is also highlighted.

REFERENCES

1. Skolnik, M. I., *Radar Handbook*, McGraw-Hill, New York, 1970.
2. Curlander, J. C. and R. N. McDounough, *Synthetic Aperture Radar, Systems and Signal Processing*, John Wiley & Sons, New York, 1991.
3. Ulaby, F. T., R. K. Moore, and A. K. Fung, *Microwave Remote Sensing: Active and Passive*, Vol. I, Artech House, Norwood, 1981.
4. Drinkwater, M. K., R. Kwok, and E. Rignot, "Synthetic aperture radar polarimetry of sea ice," *Proceeding of the 1990 International Geoscience and Remote Sensing Symposium*, Vol. 2, 1525–1528, 1990.
5. Lynne, G. L. and G. R. Taylor, "Geological assessment of SIR-B imagery of the amadeus basin," *IEEE Trans on Geosc. and Remote Sensing*, Vol. 24, No. 4, 575–581, 1986.
6. Hovland, H. A., J. A. Johannessen, and G. Digranes, "Slick detection in SAR images," *Proceeding of the 1994 International Geoscience and Remote Sensing Symposium*, 2038–2040, 1994.
7. Walker, B., G. Sander, M. Thompson, B. Burns, R. Fellerhoff, and D. Dubbert, "A high-resolution, four-band SAR Testbed with real-time image formation," *Proceeding of the 1986 International Geoscience and Remote Sensing Symposium*, 1881–1885, 1996.
8. Storvold, R., E. Malnes, Y. Larsen, K. A. Hogda, S.-E. Hamran, K. Mueller, and K. Langley, "SAR remote sensing of snow parameters in norwegian areas — Current status and future perspective," *Journal of Electromagnetic Waves and Applications*, Vol. 20, No. 13, 1751–1759, 2006.
9. Kong, J. A., S. H. Yueh, H. H. Lim, R. T. Shin, and

J. J. van Zyl, "Classification of earth terrain using polarimetric synthetic aperture radar images," *Progress In Electromagnetics Research*, PIER 03, 327–370, 1990.

10. Thompson, T. W., *A User's Guide for the NASA/JPL Synthetic Aperture Radar and the NASA/JPL L- and C-band Scatterometers*, 83–38, JPL Publication, 1986.
11. Held, D. N., W. E. Brown, A. Freeman, J. D. Klein, H. Zebker, T. Sato, T. Miller, Q. Nguyen, and Y. L. Lou, "The NASA/JPL multifrequency, multipolarisation airborne SAR system," *Proceeding of the 1988 International Geoscience and Remote Sensing Symposium*, 345–349, 1988.
12. Thompson, D. G., D. V. Arnold, and D. G. Long, "YSAR: A compact, low-cost synthetic aperture radar," *Proceeding of the 1996 International Geoscience and Remote Sensing Symposium*, 1892–1894, 1996.
13. Livingstone, C. E., A. L. Gray, R. K. Hawkins, and R. B. Olsen, "CCRS C/X-airborne synthetic aperture radar: An R&D tool for the ERS-1 time frame," *IEEE Aerospace and Electronic Systems Magazine*, Vol. 3, No. 10, 11–20, 1988.
14. Walker, B., G. Sander, M. Thompson, B. Burns, R. Fellerhoff, and D. Dubbert, "A high-resolution, four-band SAR Testbed with real-time image formation," *Proceeding of the 1986 International Geoscience and Remote Sensing Symposium*, 1881–1885, 1996.
15. Birk, R., W. Camus, E. Valenti, and W. J. McCandles, "Synthetic aperture radar imaging systems," *IEEE Aerospace and Electronic Systems Magazine*, Vol. 10, No. 11, 15–23, 1995.
16. Madsen, S. N., E. L. Christensen, N. Skou, and J. Dall, "The Danish SAR system: Design and initial tests," *IEEE Trans. on Geosc. and Remote Sensing*, Vol. 29, No. 3, 417–426, 1991.
17. Thompson, D. G., D. V. Arnold, D. G. Long, G. F. Miner, M. A. Jensen, "YINSAR: A compact, low-cost interferometric synthetic aperture radar," *Proceeding of the 1998 International Geoscience and Remote Sensing Symposium*, 1920–1922, 1998.
18. Way, J. and E. A. Smith, "The evolution of synthetic aperture radar systems and their progression to the EOS SAR," *IEEE Transactions on Geoscience and Remote Sensing*, Vol. 29, Issue 6, 962–985, 1991.
19. Nemoto, Y., H. Nishino, M. Ono, H. Mizutamari, and K. Nishikawa, K. Tanaka, "Japanese Earth Resources Satellite-1 synthetic aperture radar," *Proceedings of the IEEE*, Vol. 79, Issue 6, 800–809, 1991.

20. Jordan, R. L., B. L. Huneycutt, and M. Werner, "The SIR-C/X-SAR synthetic aperture radar system," *IEEE Transactions on Geoscience and Remote Sensing*, Vol. 33, Issue 4, 829–839, 1995.
21. Hovanessian, S. A., *Introduction to Synthetic Array and Imaging Radars*, Artech House, Dedham, 1980.
22. Kamath, J., "Real time imaging systems for synthetic aperture radar using coarse quantized correlators with VLSI realisation," Doctoral dissertation, University of Idaho, Idaho, USA, 1995.
23. Di Cenzo, A., "A new look at nonseparable synthetic aperture radar processing," *IEEE Trans. on Aerospace and Electronic Systems*, Vol. 24, No. 3, 218–223, 1988.
24. Mahafza, B. F., *Introduction to Radar Analysis*, CRC Press, New York, 1998.
25. Jakowatz, C. V., D. E. Wahl, P. H. Eichel, D. C. Ghiglia, and P. A. Thompson, *Spotlight-mode Synthetic Aperture Radar: A Signal Processing Approach*, Kluwer Academic Publishers, Boston, 1996.
26. Chan, Y., K. and S., Y. Lim, "Synthetic aperture radar (SAR) signal generation," *Progress In Electromagnetics Research B*, accepted for publication.
27. Zebker, H. A., J. J. van Zyl, and D. Held, "Imaging radar polarimetry from wave synthesis," *Journal of Geophysical Research*, Vol. 92, No. B1, 683–701, 1987.
28. Van Zyl, J. J. and H. A. Zebker, "Imaging radar polarimetry," *Progress In Electromagnetics Research*, PIER 03, 277–326, 1990.
29. Evans, D. L. and J. J. van Zyl, "Polarimetric imaging radar: Analysis tools and applications," *Progress In Electromagnetics Research*, PIER 03, 371–389, 1990.
30. Hyyppa, J., J. Pulliainen, K. Heiska, and M. Hallikainen, "Statistics of backscattering source distribution of boreal coniferous forests at C- and X-band," *Proceeding of the 1986 International Geoscience and Remote Sensing Symposium*, Vol. 1, 241–242, 1994.
31. Pulliainen, J. T., K. Heiska, J. Hyyppa, and M. T. Hallikainen, "Backscattering Properties of boreal forests at the C- and X-bands," *IEEE Trans on Geosc. and Remote Sensing*, Vol. 32, No. 5, 1041–1050, 1994.
32. Ulaby, F. T. and T. F. Bush, "Cropland inventories using an orbital imaging radar," Remote Sensing Laboratory, 1977.